Measurement of Sub-Shot-Noise Correlations of Spatial Fluctuations in the Photon-Counting Regime

Jean-Luc Blanchet, Fabrice Devaux, Luca Furfaro, and Eric Lantz

Institut FEMTO-ST, Département d'Optique PM Duffieux, UMR CNRS–Université de Franche-Comté, No. 6174, Route de Gray, 25030 Besançon Cedex, France

(Received 8 July 2008; published 3 December 2008)

We have measured sub-shot-noise quantum correlations of spatial fluctuations in the far-field image of the parametric fluorescence created in a type I beta-barium-borate nonlinear crystal. Imaging is performed at very low light level (0.15 photons per pixel) with an electron multiplying charge coupled device camera. Experimental results overcome the standard quantum limit shot-noise level without subtraction of the variance of the detection noise.

DOI: 10.1103/PhysRevLett.101.233604 PACS numbers: 42.50.Ar, 42.50.Dv

Spontaneous down-conversion (SPDC) occurs in a nonlinear crystal when a pump photon splits in a pair of signal and idler photons. Even if the number of pairs fluctuates, this relation is exact in the sense that, in the absence of input light at the signal and idler frequency, the difference between the signal and idler output photon numbers is zero in an ideal experiment. Heidmann *et al.* [1] showed that the spectrum of temporal fluctuations of the intensity difference between spatially monomode twin beams is below the standard shot-noise level. Actually, the beams are entangled: the phases of the beams are also correlated at the quantum level, as shown by homodyne detection. If the two detectors do not intercept the whole beams, the correlation is reduced because for some pairs one photon is detected while the other is not intercepted. Because ''intercepted'' can be replaced by ''detected'' in the previous sentence, such insufficient size of a detector is exactly equivalent to a reduction of the quantum efficiency. The situation is different for a strongly spatially multimode beam issued from a traveling wave amplifier: Brambilla *et al.* showed [2] that, for unity quantum efficiency, the variance of the signal-idler photon number difference goes to zero if the pixel size is much greater than the coherence area. Indeed, Boyer *et al.* studied temporal fluctuations of spatially broadband twin beams obtained by four wave mixing in a hot atomic vapor and showed that part of the beams larger than the coherence area exhibit sub-shot-noise intensity differences [3], as well as entanglement [4] if detected with local oscillators shaped as the beams. These experiments demonstrate temporal entanglement of ''subbeams'' but do not consider fluctuation of spatial variables, like position or angle. Entanglement of such variables for beams [5] has been demonstrated by combining TEM_{00} beams with a vacuum squeezed TEM_{01} beam and homodyne detection of temporal fluctuations [6]. On the other hand, Boyd *et al.* [7], demonstrated spatial entanglement of photon pairs in an image by varying the position of detectors in both the near and the far-field and recording temporal coincidences. Other spatial properties of twin photons have been extensively studied in the group of Boston [8] by recording temporal coincidences.

Though dealing with spatial aspects of multimode beams, all the experiments in the above references were devoted to the characterization of temporal fluctuations or temporal coincidences. However, patterns in an image are pure spatial information, without any time aspect, that are ultimately degraded by spatial fluctuations of quantum origin for very weak images [9]. Jedrkiewicz *et al.* [10] performed the first experimental demonstration of sub-shot-noise behavior of spatial fluctuations of the signal-idler difference. They imaged SPDC issued from a type II beta-barium-borate (BBO) crystal onto a back-illuminated charge coupled device (CCD) camera and showed that the value of the variance of the difference between signal-idler intensities on opposite pixels is below the shot-noise level. However, this result was obtained, for a mean intensity (signal + idler) of 15 photoelectrons, by subtracting the variance of the readout noise, i.e., about 100 squared photoelectrons, from a measured variance of 110 squared photoelectrons. With a conventional CCD, diminishing the relative weight of the detection noise would require the acquisition of more intense images. However, unavoidable classical noise, due, for example, to subpixel shifts between both images, becomes predominant for higher intensities as it is clearly visible in data of Ref. [10], because the variance of the classical noise scales as the square of the intensity.

We present here a more direct demonstration of sub-shot-noise correlations, without subtraction of the variance of the detector noise from the measured variance, by detecting single photons in low light level images with an electron multiplying CCD camera (EMCCD). In such cameras, the readout noise is rendered negligible by adding a register where the photoelectrons are multiplied before reading. Hence even a unique photon gives a signal that emerges from the readout floor. However, the gain is stochastic, as in an avalanche photodiode, and it is not possible to assign a precise number of photons to each

value of the output signal. It can be demonstrated [11] that dividing the output signal by the mean gain results in adding a Poisson detection noise, called excess noise, having the same amplitude as the standard photon noise. This excess noise prevents any attempt to detect sub-shot-noise correlations, at least without subtraction of the variance of the detection noise. On the other hand, for very low light level images there is either zero or one photon per pixel and detection by thresholding can be almost perfect for a high gain, even stochastic. In practice, false detections occur whose number can be minimized [12] by choosing an appropriate intensity (about 0.15 photon/pixel with our camera) and by adjusting the threshold. In these conditions, the variance of the detection noise is much smaller than the mean intensity and detection of sub-shot-noise correlations becomes possible.

The experimental setup is sketched in Fig. 1. The pump pulse provided by the fourth harmonic (0.93 ps duration at 263.8 nm) of a Q-switched mode-locked Nd:glass laser (Twinkle laser by Light Conversion, Inc.) at a repetition rate of 33 Hz, illuminated a type I $7 \times 7 \times 4$ mm^3 BBO nonlinear crystal. The far-field image of the parametric fluorescence was formed in the focal plane of a lens by a back-illuminated EMCCD camera from Andor technology (model iXon+ DU897-ECS-BV) with a quantum efficiency greater than 90% in the visible range. The detector area is formed by 512×512 pixels, with a pixel size of 16×16 μm^2. We used a readout rate of 10 MHz at 14 bit and the camera was cooled at -85 °C. The exposure time was 33 ms and the EM gain was set to 1000. In these conditions, the readout noise has a standard deviation of 46 electrons and the level of clock induced noise, i.e., generation of spurious electrons during the transfer, is of the order of $4 \times 10^{-3} e-$/pixel. A threshold set to 2.8 readout noise standard deviations allows the number of false detections to be minimized [12]. To eliminate the residual UV, two dichroic filters with a nominal transmission of 95% at 527 nm were placed after the BBO crystal. All the trajectory of the light after these dichroics was enclosed in a tube in order to avoid parasitic reflections. The energy of the 263.75 nm pump pulse was measured to 106 ± 38 nJ. The total quantum efficiency is the product of the quantum efficiency of the EMCCD by the transmission of the optical elements after the crystal.

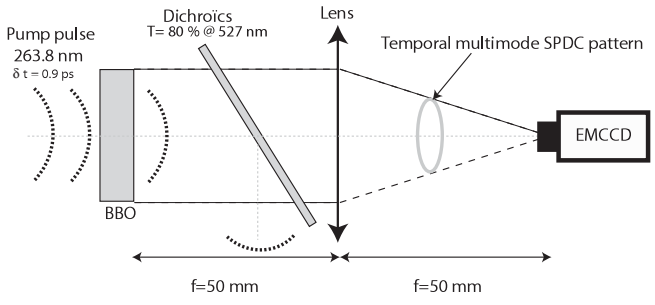

FIG. 1. Experimental setup.

$$\eta_{\mathrm{tot}} = \eta_{\mathrm{CCD}} \times \eta_{\mathrm{opt}} = 0.9 \times 0.68 = 0.62. \quad (1)$$

η_{CCD} is given by the manufacturer and η_{opt} was measured. In particular, a transmission by the two dichroic filters of 80% has been measured.

For a given crystal orientation corresponding to noncollinear phase matching and without chromatic filtering around the signal frequency, the rings corresponding to different wavelengths add incoherently in the image. As shown in Fig. 2(b), degeneracy corresponds to the smallest diameter. For nondegenerate wavelengths, the idler and signal fluorescence form rings of different diameter. However, because of momentum conservation, each pair of *twin* photons emitted in the SPDC process, although not equidistant from the center of the pattern, lie along a diameter line. We have measured the difference between the number of photons in opposite angular sectors, which should go to zero for a perfect detector and negligible diffraction, i.e., for a coherence area much smaller than the pixel size [13]. This condition is fulfilled here because of the wide illumination of the crystal: the measured pump width on the crystal (FWHM) is 3.1 mm. For pure spontaneous down-conversion with negligible further amplification and a pump beam area smaller than the crystal section (7×7 mm^2 here), the down-converted beam has the same intensity profile as the pump beam. The width of the coherence area in the far field, 0.14 mrd (FWHM), is proportional to the inverse of the width of this beam [14] and is smaller than the 0.32 mrd lateral size of the CCD pixel.

Figure 3 shows a sum of 58 single shot images of parametric fluorescence recorded by the EMCCD. Unlike in a single image, the fluorescence ring is clearly visible. The mean level in the ring for one image, about 0.15 photon per

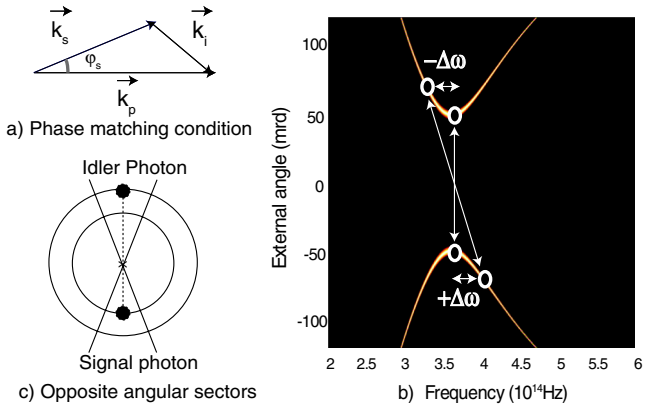

FIG. 2 (color online). (a) Noncollinear phase matching: $\vec{k}_{p,s,i}$ wave vectors of, respectively, pump, signal, idler. (b) Phase matching curves in the angle-frequency plane. The vertical arrow shows the opposite conjugate photons at the degeneracy ($\omega_i = \omega_s$): it corresponds to the smallest ring. In the nondegenerate case, idler and signal photons have symmetrical frequencies with respect to degeneracy but nonsymmetrical angles: see (a). (c) Correlation between angular sectors. For noncollinear phase matching, idler, and signal form rings of different diameters.

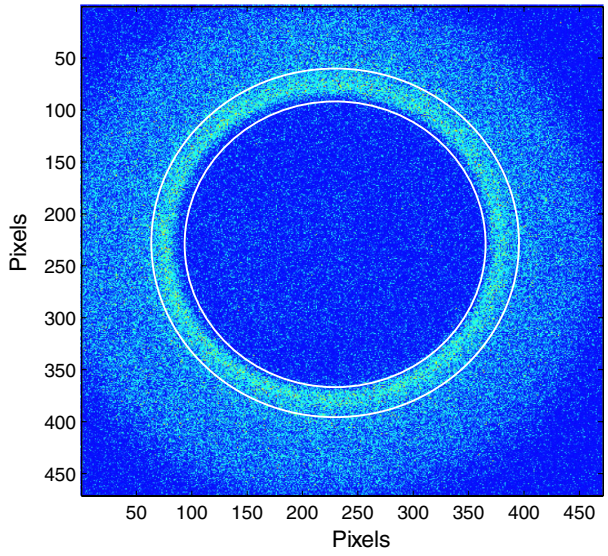

FIG. 3 (color online). Sum of 58 low light level images.

pixel, has been chosen in order to minimize the number of false detections [12]. Moreover, the mean number of photons for one spatiotemporal mode is less than 100, resulting in theoretical Bose-Einstein photon distribution [15] that is undistinguishable from a Poisson distribution. Indeed, the number of amplified temporal modes is approximately 40 [14] and the number of amplified spatial modes on a pixel is of the order of $(0.32/0.14)^2 \simeq 5$.

To take into account the nonuniform level of the electronic background over the detector area, this background is measured in darkness and subtracted from the SPDC images in the form of a mean square plane. Then, a thresholding procedure is applied on each image, in order to decide whether there is one or zero photoelectron on each pixel [12]. Note that it is not possible to distinguish the (rare) cases where two photoelectrons are present on one pixel. The SPDC image is divided in a number S of angular sectors, $S = 180$, and a number of photons n_i is determined in the intersection of each of these sectors with a ring, delimited by the white circles on Fig. 3, encompassing the greatest part of the multimode SPDC. The center of this ring is determined in order to obtain the most regular distribution of light between sectors on the sum image. Note that only the pump beam experiences walk-off, with no practical consequences since this pump beam is not detected. The size of a sector, 240 pixels, results from a compromise between effects of diffraction and not perfect centering, that are more sensitive for small sectors, and of the other classical noises (e.g., deterministic residual aberrations, see below) that predominate if the number of photons in a sector is too large. The symmetrical sector-pair correlation is evaluated by estimating the variance of the photon number difference between two opposite sectors $\sigma^2_{\mathrm{diff}} = \frac{1}{S/2-1}\sum_{i=1}^{S/2}(n_i - n_{i+S/2})^2$ and dividing this quantity either by the mean number of photons in a sector $n_{\mathrm{moy}} = \frac{1}{S}\sum_{i=1}^{S} n_i$ (black cross points on Fig. 4) or by the variance of the photon number in a sector $\sigma_s^2 = \frac{1}{S-1} \times \sum_{i=1}^{S}(n_i - n_{\mathrm{moy}})^2$ (squares). Sub-shot-noise correlation corresponds to coefficients significantly smaller than 2, value that would characterize independent sectors with Poisson photon distribution. Figure 4 shows the experimental results for 58 single shot images with a mean comprised between 0.1 and 0.25 photon/pixel: each point corresponds to a single shot measurement with a statistics performed over the 180 sectors. Results can be summarized for the whole set of images as

$$r = \frac{\sigma^2_{\mathrm{diff}}}{n_{\mathrm{moy}}} = 1.53 \pm 0.68, \qquad r' = \frac{\sigma^2_{\mathrm{diff}}}{\sigma_s^2} = 1.75 \pm 0.50. \tag{2}$$

For both values, the uncertainty range is centered on the average $\bar{r}$ or $\bar{r}'$ of the coefficients of the 58 images and the range width, i.e., ± 2 standard deviations of these 58 coefficients, gives a confidence of 95% for Gaussian measurement errors. The dispersion of the measurements of r is mainly due to the measurement of σ^2_{diff} on a limited set of 90 pairs of sectors, giving a theoretical standard deviation for Gaussian statistics equal to $(2/90)^{1/2}\sigma^2_{\mathrm{diff}}$, hence a standard deviation on r, by neglecting the much smaller uncertainty on n_{moy}: $\sigma_r = (2/90)^{1/2} r$, i.e., a theoretical uncertainty range of ± 0.45 centered on the experimental value $\bar{r} = 1.53$. The other important source of dispersion of r comes from the fluctuations of the mean photon number from an image to another due to the fluctuations of the pump energy. Though some measurement values on individual images are greater than 2, in accordance with the uncertainty range of Eq. (2), the mean coefficients are highly significantly smaller than 2:

$$\langle r \rangle = 1.53 \pm 0.09, \qquad \langle r' \rangle = 1.75 \pm 0.07. \tag{3}$$

The uncertainty range on the mean coefficients in Eq. (3) is obtained by dividing the uncertainty on each image in Eq. (2) by the square root of the image number ($\sqrt{58}$). The

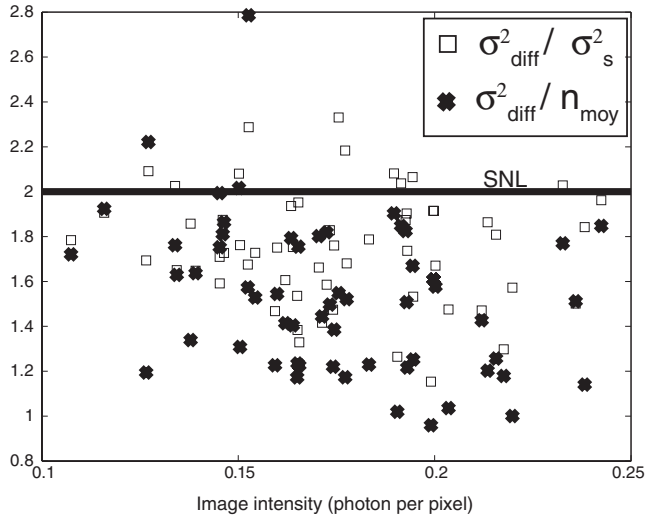

FIG. 4. Experimental results: each point corresponds to a single shot measurement.

most reliable result is given by the coefficient $\langle r' \rangle$; indeed, the variance of the photon number in a sector appears to be smaller than the mean photon number, while the equality is expected for a Poisson distribution. This phenomenon can be easily explained by taking into account the cases where two photoelectrons or more are accumulated in the same pixel. If μ is the true mean number of photoelectrons accumulated in one pixel, a thresholding procedure would give, in the absence of false detections, a measured mean m given by

$$m = 1 - p(0) = 1 - \exp(-\mu), \tag{4}$$

where p(0) is the probability of detecting no photoelectron. The first equality expresses the fact that the thresholding procedure is unable to distinguish between one and more photoelectrons on one pixel, while the second equality reflects the Poisson distribution of photoelectrons. With the same hypotheses, the measured variance v is given by

$$v = m^2 p(0) + (1 - m)^2 (1 - p(0)) = m(1 - m). \tag{5}$$

Hence, the measured variance is smaller than the measured mean, because of the binary detection. On the other hand, the variance of the difference is affected in the same way as the variance by this effect and the ratio between these variances gives an estimation of quantum correlations, with a standard quantum limit equal to 2. By using this ratio, we have therefore demonstrated experimental quantum correlations between opposite sectors, with neither corrections or artifacts due to the detector. The other detector errors are false detections of one photon when there is none, and no detection of an incident photon, because of either the nonunity quantum efficiency or the nonzero value of the threshold [12]. Both errors deteriorate quantum correlations.

We have calculated the spatial distribution of quantum fluctuations of SPDC by using the Green's function method described in [13] and including a realistic model of the EMCCD camera. With this model, we obtain

$$r' = \frac{\sigma^2_{\mathrm{diff}}}{\sigma^2_s} = 1.33. \tag{6}$$

For a perfect detector, the ratio value is 0.57, with a weak contribution of diffraction, because the size of the coherence area is much smaller than the pixel size [13]. Almost all the loss before detection of one photon in a pair is due to noncollinear phase matching, in the cases where the signal ring is included in the detection area while the idler ring is outside this area. If the detection was perfect, such a situation could be avoided by extending the outer diameter of the detection ring. However, in practice, experimental results are worse because of the contribution of the detector noise in the low intensity part of this area. A part of the remaining difference between experiment ($r' = 1.75$) and theory ($r' = 1.33$) is due to deterministic aberrations. Indeed the photon number values in the angular sectors determined on the sum of the 58 images have a deterministic part depending of the angle. After division by the number of images, the value of this deterministic signal is much weaker than the quantum random signal but non-negligible, and leads to an increase of r of about 0.1. Nevertheless, a discrepancy remains, whose origin is not clear. Note, however, that parametric amplifiers are often described in quantum optics by introducing an ''excess noise'' factor [16], whose origin comes from distortions in the pump wave front.

In conclusion, we have experimentally demonstrated that opposite spatial fluctuations of spontaneous down-conversion radiation are correlated in the quantum regime. The variance of the photon number difference between opposite sectors is equal to $\langle r' \rangle = 1.75 \pm 0.07 \times$ the variance between sectors (at 95% of confidence), i.e., clearly below the quantum limit of 2 for Poisson noise. This coefficient is issued directly of our measures: the variance due to detection noise has not been subtracted of the experimental measured variance. The next step will consist in demonstrating true ''spatial coincidences'' for pair of photons on opposite pixels, by using chromatic filtering around degeneracy.

This work has been supported by the Agence Nationale pour la Recherche, project IRCOQ.

[1] A. Heidmann, R. J. Horowicz, S. Reynaud, E. Giacobino, C. Fabre, and G. Camy, Phys. Rev. Lett. **59**, 2555 (1987).
[2] E. Brambilla, A. Gatti, M. Bache, and L. A. Lugiato, Phys. Rev. A **69**, 023802 (2004).
[3] V. Boyer, A. M. Marino, and P. D. Lett, Phys. Rev. Lett. **100**, 143601 (2008).
[4] V. Boyer, A. M. Marino, R. C. Pooser, and P. D. Lett, Science **321**, 544 (2008).
[5] M. T. L Hsu, W. P. Bowen, N. Treps, and P. K. Lam, Phys. Rev. A **72**, 013802 (2005).
[6] K. Wagner *et al.*, Science **321**, 541 (2008).
[7] J. C. Howell, R. S. Bennink, S. J. Bentley, and R. W. Boyd, Phys. Rev. Lett. **92**, 210403 (2004).
[8] D. V. Strekalov, A. V. Sergienko, D. N. Klyshko, and Y. H. Shih, Phys. Rev. Lett. **74**, 3600 (1995).
[9] A. Mosset, F. Devaux, and E. Lantz, Phys. Rev. Lett. **94**, 223603 (2005).
[10] O. Jedrkiewicz, Y.-K Jiang, E. Brambilla, A. Gatti, M. Bache, L. A. Lugiato, and P. Di Trapani, Phys. Rev. Lett. **93**, 243601 (2004).
[11] J. Hynecek and T. Nishiwaki, IEEE Trans. Electron Devices **50**, 239 (2003)
[12] E. Lantz, J. L Blanchet, L. Furfaro, and F. Devaux, Mon. Not. R. Astron. Soc. **386**, 2262 (2008).
[13] E. Lantz, N. Treps, C. Fabre, and E. Brambilla, Eur. Phys. J. D **29**, 437 (2004).
[14] F. Devaux and E. Lantz, Eur. Phys. J. D **8**, 117 (2000).
[15] A. Mosset, F. Devaux, G. Fanjoux, and E. Lantz, Eur. Phys. J. D **28**, 447 (2004).
[16] A. Ourjoumtsev, R. Tualle-Brouri, J. Laurat, and P. Grangier, Science **312**, 83 (2006).